# PARKER-JEANS INSTABILITY OF GASEOUS DISKS INCLUDING THE EFFECT OF COSMIC RAYS

## Takuhito Kuwabara

Applied Research and Standards Department, National institute of Information and Communications Technology, Koganei, Tokyo 184-8795, Japan

kuwabrtk@cc.nao.ac.jp

and

Chung-Ming Ko

Department of Physics, Institute of Astronomy and Center for Complex Systems, National Central University, Chung-Li, Taiwan 320, Republic of China

cmko@astro.ncu.edu.tw

#### ABSTRACT

We use linear analysis to examine the effect of cosmic rays (CRs) on the Parker-Jeans instability of magnetized self-gravitating gaseous disks. We adopt a slab equilibrium model in which the gravity (including self-gravity) is perpendicular to the mid-plane, the magnetic field lies along the slab. CR is described as a fluid and only along magnetic field lines diffusion is considered. The linearised equations are solved numerically. The system is susceptible to Parker-Jeans instability. In general the system is less unstable when the CR diffusion coefficient is smaller (i.e., the coupling between the CRs and plasma is stronger). The system is also less unstable if CR pressure is larger. This is a reminiscence of the fact that Jeans instability and Parker instability are less unstable when the gas pressure is larger (or temperature is higher). Moreover, for large CR diffusion coefficient (or small CR pressure), perturbations parallel to the magnetic field are more unstable than those perpendicular to it. The other governing factor on the growth rate of the perturbations in different directions is the thickness of the disk or the strength of the external pressure on the disk. In fact, this is the determining factor in some parameter regimes.

Subject headings: cosmic rays — instabilities — ISM: magnetic fields — MHD

#### 1. INTRODUCTION

In our Galaxy (and probably other galaxies as well), the energy densities of thermal gas, magnetic field, cosmic rays and turbulence are of the same order of magnitude (~1 eV cm<sup>-3</sup>, see e.g., Gaisser 1990). Rough equipartition exists between these components indicates that they are tightly coupled together, and all of them should have significant influence on the structure and evolution of the interstellar medium (ISM). However, the dynamical role of CRs on ISM has not been taken seriously in most ISM related models until rather recently (see e.g., Ferrière 2001).

The ISM is highly inhomogeneous and have many different phases of gas clouds, e.g., hot phase, warm phase, diffuse clouds, molecular clouds, etc. This is due partly to the existence of many instabilities in ISM conditions. Gravitational instability (Jeans instability) and magnetic buoyancy instability (Parker instability, Parker 1966) have been considered to be responsible for the formation of some large scale clouds (e.g., HI clouds, molecular clouds). As ISM is aggregated, filament-like structures are formed by Parker-Jeans instability. Extensive analytical works on Parker-Jeans instability have been carried out in the past two to three decades (e.g., Elmegreen & Elmegreen 1978; Elmegreen 1982a,b; Hanawa et al. 1992; Nagai et al. 1998; Lee & Hong 2005). Recently, this instability has been studied by the magnetohydrodynamic (MHD) simulations (e.g., Chou et al. 2000; Lee et al. 2001; Kim et al. 2002). Nagai et al. (1998) showed that the angle of the filament formed by this instability with respect to the magnetic field lines depends on the strength of the external gas pressure of the initial equilibrium gas layer, and Chou et al. (2000) confirmed their results by MHD simulations. Nevertheless, the dynamical effect of CRs has not been addressed in these works.

In his original work on the Parker instability, Parker realised the importance of CRs on the instability and did consider their effect in a simplified way (Parker 1966). However, studies on the instability with more rigorous treatment of the dynamics of CRs appear only rather recently. Both linear analysis (Kim et al. 1997; Kim & Hong 1998; Hanasz & Lesch 1997; Hanasz 1997; Ryu et al. 2003) and MHD simulation (Hanasz & Lesch 2000, 2003; Hanasz et al. 2004a,b; Kuwabara et al. 2004) have been performed on models in which the diffusion of CRs through plasma is included. These models are based on the hydrodynamic description of CRs (e.g., Drury & Völk 1981; Drury 1983; Ko 1992), which is a fairly good approximation in studying the structure and evolution of the system, although the spectrum of CR is compromised. As far as we know, the effect of the CR diffusion on the Parker-Jeans instability has not been studied yet.

In this paper, the effect of CRs on the Parker-Jeans instability is examined by linear analysis. Hydrodynamic approach to CR is adopted and only along field line diffusion is

considered. As a model for Galactic gaseous disk or compressed molecular cloud, a self-gravitating gas layer or slab threaded by magnetic field perpendicular to the gravity is used for the unperturbed equilibrium state. The dispersion relations are obtained numerically. The paper is organised as follows. In  $\S 2$ , we present the CR-plasma system and the equilibrium model.  $\S 3$  is devoted to linear stability analysis, and the results are described in  $\S 4$ .  $\S 5$  provides a summary and discussion.

#### 2. MODELS

## 2.1. Two-Fluid Model

We adopt a two-fluid model which comprises cosmic rays and thermal gas (e.g., Drury & Völk 1981; Drury 1983; Ko 1992). CR is treated as a massless gas with significant energy density or pressure. CRs are coupled to the thermal gas via hydromagnetic irregularities or waves embedded in the flow. To a first approximation, the only effect of the irregularities or waves is contained in the diffusion coefficient of CR. For simplicity, we consider diffusion along magnetic field lines only and ignore the cross-field-line diffusion (see e.g., Giacalone & Jokipii 1999). Thus  $\kappa = \kappa_{\parallel} \mathbf{b} \mathbf{b}$ , where  $\mathbf{b}$  is the unit vector along the magnetic field.

Assuming infinite conductivity for the plasma (i.e., ideal MHD), the system is governed by the total mass equation, momentum equation, thermal and CR energy equations,

$$\frac{\partial \rho}{\partial t} + \nabla \cdot (\rho \mathbf{V}) = 0, \qquad (1)$$

$$\frac{\partial}{\partial t} (\rho \mathbf{V}) + \nabla \cdot \left[ \rho \mathbf{V} \mathbf{V} + \left( P_{g} + P_{c} + \frac{B^{2}}{2\mu_{0}} \right) \mathbf{I} - \frac{\mathbf{B} \mathbf{B}}{\mu_{0}} \right] 
+ \rho \left[ \nabla (\psi + \psi_{e}) + 2\mathbf{\Omega} \times \mathbf{V} + \mathbf{\Omega} \times (\mathbf{\Omega} \times \mathbf{r}) \right] = 0,$$
(2)

$$\frac{\partial P_{g}}{\partial t} + \mathbf{V} \cdot \nabla P_{g} + \gamma_{g} P_{g} \nabla \cdot \mathbf{V} = 0, \qquad (3)$$

$$\frac{\partial P_{c}}{\partial t} + \mathbf{V} \cdot \nabla P_{c} + \gamma_{c} P_{c} \nabla \cdot \mathbf{V} - \nabla \cdot \left( \kappa_{\parallel} \mathbf{b} \mathbf{b} \cdot \nabla P_{c} \right) = 0, \tag{4}$$

supplemented by the Poisson equation for self-gravity and induction equation for magnetic field

$$\nabla^2 \psi = 4\pi G \rho \,, \tag{5}$$

$$\frac{\partial \mathbf{B}}{\partial t} = \nabla \times (\mathbf{V} \times \mathbf{B}), \qquad (6)$$

$$\nabla \cdot \mathbf{B} = 0. \tag{7}$$

In these equations  $\rho$ ,  $\mathbf{V}$ ,  $P_{\rm g}$  and  $\gamma_{\rm g}$  denote the thermal gas density, flow velocity, pressure and polytropic index, respectively;  $P_{\rm c}$ ,  $\gamma_{\rm c}$  and  $\kappa_{\parallel}$  denote the CR pressure, polytropic index and diffusion coefficient along magnetic field lines, respectively;  $\psi$  and  $\psi_{\rm e}$  denote the potential of the self-gravity of the gas and the potential of some external gravitational source, respectively;  $\mathbf{B}$  is the magnetic field strength and  $\mathbf{\Omega}$  is the angular velocity of the disk. In the rest of the paper we assume that the centrifugal force is balanced by the external gravitational source.

## 2.2. Equilibrium Model

We are interested in the stability of a uniformly rotating gaseous disk or a slab. We adopt a local Cartesian coordinate system (x, y, z) such that  $\mathbf{e_x} = \mathbf{e_\phi}$ ,  $\mathbf{e_y} = -\mathbf{e_r}$  and  $\mathbf{e_z} = \mathbf{e_z}$ , where  $(r, \phi, z)$  is the cylindrical coordinate system of the disk. All quantities of the unperturbed equilibrium state depend on z only. Moreover, assume initial magnetic field is in the azimuthal direction, i.e.,  $\mathbf{B} = B(z)\mathbf{e_x}$ . For simplicity ignore the external gravitational force in the z-direction, the equilibrium model satisfies the magnetohydrostatic equation

$$\frac{\mathrm{d}}{\mathrm{d}z} \left( P_{\mathrm{g}} + P_{\mathrm{c}} + \frac{B^2}{2\mu_0} \right) + \rho \frac{\mathrm{d}\psi}{\mathrm{d}z} = 0. \tag{8}$$

Substitute into the Poisson equation (Eq. (5)), we obtain

$$\frac{\mathrm{d}}{\mathrm{d}z} \left[ \frac{C_{\mathrm{s}}^{2} (1 + \alpha + \beta)}{\gamma_{\mathrm{g}} P_{\mathrm{t}}} \frac{\mathrm{d}P_{\mathrm{t}}}{\mathrm{d}z} \right] + \frac{4\pi G \gamma_{\mathrm{g}} P_{\mathrm{t}}}{C_{\mathrm{s}}^{2} (1 + \alpha + \beta)} = 0, \qquad (9)$$

where  $\alpha$  and  $\beta$  are the ratio of the magnetic pressure and CR pressure to the gas pressure,  $P_{\rm t}=(1+\alpha+\beta)P_{\rm g}$  is the total pressure, and  $C_{\rm s}=(\gamma_{\rm g}P_{\rm g}/\rho)^{1/2}$  is the gas sound speed. Moreover, we assume a temperature distribution

$$T(z) = \begin{cases} T_d, & \text{for } |z| < z_d, \\ \infty, & \text{for } |z| > z_d, \end{cases}$$
 (10)

(Hanawa et al. 1992), where  $T_d$  and  $z_d$  are the temperature and the half-thickness of the (cold) gaseous disk. Large (small)  $z_d$  can be interpreted as small (large) external pressure. Integrate Eq. (9) with this temperature distribution gives the equilibrium pressure and density distributions. The density scale height at z=0 (mid-plane of the gaseous disk) is  $H=C_{\rm s0}\sqrt{(1+\alpha+\beta)/(2\pi G\rho_0\gamma_{\rm g})}$ , where the subscript 0 denotes the value at the mid-plane. Naturally, we normalise the density, velocity and length of the gaseous disk to  $\rho_0$ ,  $C_{\rm s0}$  and  $H_0=C_{\rm s0}/\sqrt{2\pi G\rho_0\gamma_{\rm g}}$ . The CR diffusion coefficient is normalised to  $C_{\rm s0}H_0$ . In this paper we choose  $\gamma_{\rm g}=1$  and  $\gamma_{\rm c}=4/3$ . We pick  $\alpha=1$ ,  $\beta=1$  and  $z_d=H_0$  as the fiducial model.

Fig. 1 shows the distribution of the equilibrium gas pressure and the gravity in the case of  $\alpha = 1$  and  $\beta = 1$ .

Parker-Jeans instability is one of the possible mechanisms for the formation of large ISM clouds (e.g., molecular clouds, HI clouds), thus the typical values for  $\rho_0$ ,  $C_{\rm s0}$ ,  $H_0$  and  $C_{\rm s0}H_0$  are  $1.67\times 10^{-21}$  kg m<sup>-3</sup>, 5 km s<sup>-1</sup>, 200 pc and  $3\times 10^{22}$  m<sup>2</sup> s<sup>-1</sup>. The effective sound speed  $C_{\rm s0}\sqrt{1+\alpha+\beta}\sim 8.5$  km s<sup>-1</sup> for  $\alpha=\beta=1$  (Hanawa et al. 1992). The value of CR diffusion coefficient is estimated to be  $3\times 10^{24}$  m<sup>2</sup> s<sup>-1</sup> (e.g., Brezzinskii et al. 1990; Ptuskin 2001; Ryu et al. 2003). Thus the fiducial value of normalised  $\kappa_{\parallel}$  is 100. On the other hand, Parker-Jeans instability may cause the fragmentation and collapse of large ISM clouds. The typical values for  $\rho_0$ ,  $C_{\rm s0}$ ,  $H_0$  and  $C_{\rm s0}H_0$  become  $1.67\times 10^{-19}$  kg m<sup>-3</sup>, 5 km s<sup>-1</sup>, 20 pc and  $3\times 10^{21}$  m<sup>2</sup> s<sup>-1</sup>. In this case the CR diffusion coefficient is smaller, say  $3\times 10^{23}$  m<sup>2</sup> s<sup>-1</sup>, then the fiducial value of normalised  $\kappa_{\parallel}$  is still 100.

#### 3. LINEAR STABILITY ANALYSIS

## 3.1. Equations for Perturbations

We perform standard linear stability analysis on the system of equations Eqs. (1)-(7) of the slab equilibrium model described in previous section. Since the unperturbed state depends on z only, we assume the perturbed quantities to be of the following form

$$\begin{bmatrix} \delta \rho \\ \delta V_{x} \\ \delta V_{y} \\ \delta V_{z} \\ \delta P_{g} \\ \delta P_{c} \\ \delta B_{x} \\ \delta B_{y} \\ \delta B_{z} \\ \delta \psi \end{bmatrix} = \begin{bmatrix} \delta \bar{\rho} \\ i \delta \bar{V}_{x} \\ i \delta \bar{V}_{y} \\ \delta \bar{V}_{z} \\ \delta \bar{P}_{g} \\ \delta \bar{P}_{c} \\ \delta \bar{B}_{x} \\ \delta \bar{B}_{y} \\ -i \delta \bar{B}_{z} \\ \delta \bar{\psi} \end{bmatrix} \exp(\sigma t + i k_{x} x + i k_{y} y), \qquad (11)$$

where the barred quantities are functions of z only,  $\sigma$  is the growth rate, and  $k_x$ ,  $k_y$  are the wave numbers in the x- and y-directions, respectively. The set of linearised equations becomes

$$\sigma \frac{\delta \bar{\rho}}{\rho} - k_x \delta \bar{V}_x - k_y \delta \bar{V}_y + \frac{\mathrm{d}\delta \bar{V}_z}{\mathrm{d}z} + \frac{1}{\rho} \frac{\mathrm{d}\rho}{\mathrm{d}z} \delta \bar{V}_z = 0, \qquad (12)$$

$$\sigma \delta \bar{V}_x + \frac{k_x}{\rho} \delta \bar{P}_g + \frac{k_x}{\rho} \delta \bar{P}_c + \frac{1}{\mu_0 \rho} \frac{\mathrm{d}B_x}{\mathrm{d}z} \delta \bar{B}_z - 2\Omega \delta \bar{V}_y + k_x \delta \bar{\psi} = 0, \qquad (13)$$

$$\sigma \delta \bar{V}_y + \frac{k_y}{\rho} \delta \bar{P}_g + \frac{k_y}{\rho} \delta \bar{P}_c - \frac{k_x B}{\mu_0 \rho} \delta \bar{B}_y + \frac{k_y B}{\mu_0 \rho} \delta \bar{B}_x + 2\Omega \delta \bar{V}_x + k_y \delta \bar{\psi} = 0, \qquad (14)$$

$$\sigma \delta \bar{V}_z + \frac{1}{\rho} \frac{\mathrm{d}\delta \bar{P}_g}{\mathrm{d}z} + \frac{1}{\rho} \frac{\mathrm{d}\delta \bar{P}_c}{\mathrm{d}z} + \frac{1}{\rho} \frac{\mathrm{d}}{\mathrm{d}z} \left( \frac{B \delta \bar{B}_x}{\mu_0} \right) - \frac{k_x B}{\mu_0 \rho} \delta \bar{B}_z$$
$$-\frac{1}{\rho^2} \frac{\mathrm{d}}{\mathrm{d}z} \left( P_g + P_c + \frac{B^2}{2\mu_0} \right) + \frac{\mathrm{d}\delta \bar{\psi}}{\mathrm{d}z} = 0, \tag{15}$$

$$\sigma \delta \bar{P}_{g} + \frac{dP_{g}}{dz} \delta \bar{V}_{z} - \frac{\gamma_{g} P_{g}}{\rho} \left( \sigma \delta \bar{\rho} + \frac{d\rho}{dz} \delta \bar{V}_{z} \right) = 0, \qquad (16)$$

$$\sigma \delta \bar{P}_{c} + \frac{dP_{c}}{dz} \delta \bar{V}_{z} - \frac{\gamma_{c} P_{c}}{\rho} \left( \sigma \delta \bar{\rho} + \frac{d\rho}{dz} \delta \bar{V}_{z} \right) + \kappa_{\parallel} k_{x}^{2} \delta \bar{P}_{c} - \frac{\kappa_{\parallel} k_{x}}{B} \frac{dP_{c}}{dz} \delta \bar{B}_{z} = 0, \quad (17)$$

$$-(k_x^2 + k_y^2)\delta\bar{\psi} + \frac{\mathrm{d}^2\delta\psi}{\mathrm{d}z^2} - 4\pi G\delta\bar{\rho} = 0, \qquad (18)$$

$$\sigma \delta \bar{B}_x + k_x B \delta \bar{V}_x + \frac{\mathrm{d}B}{\mathrm{d}z} \delta \bar{V}_z - \frac{B}{\rho} \left( \sigma \delta \bar{\rho} + \frac{\mathrm{d}\rho}{\mathrm{d}z} \delta \bar{V}_z \right) = 0, \tag{19}$$

$$\sigma \delta \bar{B}_y + k_x B \delta \bar{V}_y = 0 \,, \tag{20}$$

$$\sigma \delta \bar{B}_z + k_x B \delta \bar{V}_z = 0 \,, \tag{21}$$

$$k_x \delta \bar{B}_x + k_y \delta \bar{B}_y - \frac{\mathrm{d}\delta \bar{B}_z}{\mathrm{d}z} = 0. \tag{22}$$

After some manipulations, we obtain the following set of ordinary differential equations,

$$\frac{\mathrm{d}}{\mathrm{d}z} \begin{bmatrix} y_1 \\ y_2 \\ y_3 \\ y_4 \end{bmatrix} = \begin{bmatrix} A_{11} & A_{12} & A_{13} & 0 \\ A_{21} & A_{22} & A_{23} & A_{24} \\ 0 & 0 & 0 & -1 \\ A_{41} & A_{42} & A_{43} & 0 \end{bmatrix} \cdot \begin{bmatrix} y_1 \\ y_2 \\ y_3 \\ y_4 \end{bmatrix},$$
(23)

where the running variables are defined as

$$y_1 \equiv -\frac{\rho \delta \bar{V}_z}{\sigma} \,, \tag{24}$$

$$y_2 \equiv \delta \bar{P}_{\rm t} = \delta \bar{P}_{\rm g} + \delta \bar{P}_{\rm c} + \frac{B}{\mu_0} \delta \bar{B}_x \,, \tag{25}$$

$$y_3 \equiv \delta \bar{\psi} \,, \tag{26}$$

$$y_4 \equiv \delta \bar{g}_z = -\frac{\mathrm{d}\delta \bar{\psi}}{\mathrm{d}z}, \qquad (27)$$

and the matrix elements are

$$A_{11} = \left[1 - \frac{\sigma^{2}}{\Sigma^{2}} - \frac{V_{A}^{2}k_{x}^{2}}{\Sigma^{2}(1 + \Gamma^{2})} \left(\Gamma^{2} + \frac{k_{y}}{k_{x}}\Gamma\right)\right] \frac{\mathrm{d}\ln\rho}{\mathrm{d}z}$$

$$-\frac{1}{D} \left[\frac{\sigma^{2}}{\Sigma^{2}} + \frac{V_{A}^{2}k_{x}^{2}}{\Sigma^{2}(1 + \Gamma^{2})} \left(\Gamma^{2} + \frac{k_{y}}{k_{x}}\Gamma\right)\right]$$

$$\times \left\{V_{A}^{2} \frac{\mathrm{d}\ln B}{\mathrm{d}z} + \frac{1}{\rho} \frac{\mathrm{d}P_{c}}{\mathrm{d}z} - \left\{\frac{C_{c}^{2}}{(1 + K)} + V_{A}^{2} \left[\frac{\sigma^{2}}{\Sigma^{2}} + \frac{k_{x}^{2}V_{A}^{2}\Gamma^{2}}{\Sigma^{2}(1 + \Gamma^{2})}\right]\right\} \frac{\mathrm{d}\ln\rho}{\mathrm{d}z}\right\}, \quad (28)$$

$$A_{12} = \frac{(k_x^2 + k_y^2)}{\Sigma^2 (1 + \Gamma^2)} + \frac{1}{D} \left[ \frac{\sigma^2}{\Sigma^2} + \frac{V_A^2 k_x^2}{\Sigma^2 (1 + \Gamma^2)} \left( \Gamma^2 + \frac{k_y}{k_x} \Gamma \right) \right] \times \left[ \frac{\sigma^2}{\Sigma^2} + \frac{V_A^2 k_x^2}{\Sigma^2 (1 + \Gamma^2)} \left( \Gamma^2 - \frac{k_y}{k_x} \Gamma \right) \right], \tag{29}$$

$$A_{13} = \frac{(k_x^2 + k_y^2)\rho}{\Sigma^2(1 + \Gamma^2)} - \frac{1}{D} \frac{V_A^2 k_x^2 \rho}{\Sigma^2(1 + \Gamma^2)} \left(1 + \frac{k_y}{k_x} \Gamma\right) \left[\frac{\sigma^2}{\Sigma^2} + \frac{V_A^2 k_x^2}{\Sigma^2(1 + \Gamma^2)} \left(\Gamma^2 + \frac{k_y}{k_x} \Gamma\right)\right], \quad (30)$$

$$A_{21} = \sigma^{2} + V_{A}^{2} k_{x}^{2} - \frac{g_{z}}{D} \left\{ V_{A}^{2} \frac{\mathrm{d} \ln B}{\mathrm{d} z} + \frac{1}{\rho} \frac{\mathrm{d} P_{c}}{\mathrm{d} z} - \left\{ \frac{C_{c}^{2}}{(1+K)} + V_{A}^{2} \left[ \frac{\sigma^{2}}{\Sigma^{2}} + \frac{k_{x}^{2} V_{A}^{2} \Gamma^{2}}{\Sigma^{2} (1+\Gamma^{2})} \right] \right\} \frac{\mathrm{d} \ln \rho}{\mathrm{d} z} \right\},$$
(31)

$$A_{22} = \frac{g_z}{D} \left[ \frac{\sigma^2}{\Sigma^2} + \frac{V_{\rm A}^2 k_x^2}{\Sigma^2 (1 + \Gamma^2)} \left( \Gamma^2 - \frac{k_y}{k_x} \Gamma \right) \right] , \tag{32}$$

$$A_{23} = -\frac{g_z}{D} \frac{V_A^2 k_x^2 \rho}{\Sigma^2 (1 + \Gamma^2)} \left( 1 + \frac{k_y}{k_x} \Gamma \right) , \qquad (33)$$

$$A_{24} = \rho \,, \tag{34}$$

$$A_{41} = \frac{4\pi G}{D} \left\{ V_{\rm A}^2 \frac{\mathrm{d} \ln B}{\mathrm{d} z} + \frac{1}{\rho} \frac{\mathrm{d} P_{\rm c}}{\mathrm{d} z} - \left\{ \frac{C_{\rm c}^2}{(1+K)} + V_{\rm A}^2 \left[ \frac{\sigma^2}{\Sigma^2} + \frac{k_x^2 V_{\rm A}^2 \Gamma^2}{\Sigma^2 (1+\Gamma^2)} \right] \right\} \frac{\mathrm{d} \ln \rho}{\mathrm{d} z} \right\}, \quad (35)$$

$$A_{42} = -\frac{4\pi G}{D} \left[ \frac{\sigma^2}{\Sigma^2} + \frac{V_A^2 k_x^2}{\Sigma^2 (1 + \Gamma^2)} \left( \Gamma^2 - \frac{k_y}{k_x} \Gamma \right) \right] , \qquad (36)$$

$$A_{43} = -(k_x^2 + k_y^2) + \frac{4\pi G}{D} \frac{V_A^2 k_x^2 \rho}{\Sigma^2 (1 + \Gamma^2)} \left( 1 + \frac{k_y}{k_x} \Gamma \right) , \qquad (37)$$

in which

$$K = \frac{\kappa_{\parallel} k_x^2}{\sigma}, \quad \Sigma^2 = \sigma^2 + V_A^2 k_x^2, \quad \Gamma = \frac{2\sigma\Omega}{\Sigma^2},$$

$$D = C_s^2 + \frac{C_c^2}{(1+K)} + V_A^2 \left[ \frac{\sigma^2}{\Sigma^2} + \frac{V_A^2 k_x^2 \Gamma^2}{\Sigma^2 (1+\Gamma^2)} \right], \quad (38)$$

$$C_{\rm s}^2 = \frac{\gamma_{\rm g} P_{\rm g}}{\rho}, \quad C_{\rm c}^2 = \frac{\gamma_{\rm c} P_{\rm c}}{\rho}, \quad V_A^2 = \frac{B^2}{\mu_0 \rho}, \quad g_z = \frac{1}{\rho} \frac{\mathrm{d} P_{\rm t}}{\mathrm{d} z}.$$
 (39)

For completeness, we list the perturbed quantities in terms of the running variables (24)-(27),

$$\delta \bar{\rho} = -\left\{ V_{\rm A}^2 \frac{\mathrm{d} \ln B}{\mathrm{d} z} + \frac{1}{\rho} \frac{\mathrm{d} P_{\rm c}}{\mathrm{d} z} - \left\{ \frac{C_{\rm c}^2}{(1+K)} + V_{\rm A}^2 \left[ \frac{\sigma^2}{\Sigma^2} + \frac{k_x^2 V_{\rm A}^2 \Gamma^2}{\Sigma^2 (1+\Gamma^2)} \right] \right\} \frac{\mathrm{d} \ln \rho}{\mathrm{d} z} \right\} \frac{y_1}{D} + \left[ \frac{\sigma^2}{\Sigma^2} + \frac{V_{\rm A}^2 k_x^2}{\Sigma^2 (1+\Gamma^2)} \left( \Gamma^2 - \frac{k_y}{k_x} \Gamma \right) \right] \frac{y_2}{D} - \frac{V_{\rm A}^2 k_x^2 \rho}{\Sigma^2 (1+\Gamma^2)} \left( 1 + \frac{k_y}{k_x} \Gamma \right) \frac{y_3}{D}, \tag{40}$$

$$\delta \bar{V}_x = -\frac{\sigma k_x}{\Sigma^2 (1 + \Gamma^2)} \left[ \left( 1 + \frac{k_y}{k_x} \right) \left( y_3 + \frac{y_2}{\rho} \right) + V_A^2 \left( \frac{1}{\rho^2} \frac{\mathrm{d}\rho}{\mathrm{d}z} y_1 - \frac{\delta \bar{\rho}}{\rho} \right) \right] , \tag{41}$$

$$\delta \bar{V}_y = -\frac{\sigma k_y}{\Sigma^2 (1 + \Gamma^2)} \left[ \left( 1 + \frac{k_x}{k_y} \right) \left( y_3 + \frac{y_2}{\rho} \right) + V_A^2 \Gamma \frac{k_x}{k_y} \left( \frac{1}{\rho^2} \frac{\mathrm{d}\rho}{\mathrm{d}z} y_1 - \frac{\delta \bar{\rho}}{\rho} \right) \right] , \tag{42}$$

$$\delta \bar{V}_z = -\frac{\sigma}{\rho} y_1 \,, \tag{43}$$

$$\delta \bar{P}_{g} = C_{s}^{2} \delta \bar{\rho} - \frac{1}{\rho} \left( C_{s}^{2} \frac{\mathrm{d}\rho}{\mathrm{d}z} - \frac{\mathrm{d}P_{g}}{\mathrm{d}z} \right) y_{1}, \tag{44}$$

$$\delta \bar{P}_{c} = \frac{C_{c}^{2}}{(1+K)} \delta \bar{\rho} - \frac{1}{\rho} \left[ \frac{C_{c}^{2}}{(1+K)} \frac{\mathrm{d}\rho}{\mathrm{d}z} - \frac{\mathrm{d}P_{c}}{\mathrm{d}z} \right] y_{1}, \tag{45}$$

$$\delta \bar{\psi} = y_3 \,, \qquad \delta \bar{g}_z = y_4 \,, \tag{46}$$

$$\delta \bar{B}_x = \frac{B}{\rho} \left( \frac{\mathrm{d} \ln B}{\mathrm{d} z} - \frac{\mathrm{d} \ln \rho}{\mathrm{d} z} \right) y_1 + B \frac{\delta \bar{\rho}}{\rho} - \frac{k_x}{\sigma} B \delta \bar{V}_x \,, \tag{47}$$

$$\delta \bar{B}_y = -\frac{k_x}{\sigma} B \delta \bar{V}_y \,, \tag{48}$$

$$\delta \bar{B}_z = -\frac{k_x}{\sigma} B_x \delta \bar{V}_z \,, \tag{49}$$

By setting up suitable boundary conditions at z = 0 and  $z = z_d$ , the set of equations (Eq. (23)) is solved for given  $(k_x, k_y)$ . The growth rate is the corresponding eigenvalue that satisfies the boundary conditions.

## 3.2. Boundary Conditions

The slab geometry and layered equilibrium model (Eq. (10)) we use in §2 is a kind of disk-halo model. We adopt the boundary conditions used by Nagai et al. (1998), Hanawa et al. (1992) and Chou et al. (2000) for the interface between disk and halo (at  $z = z_d$ ). The

boundary conditions are derived from the continuity of velocity, pressure, magnetic field, gravitational potential, and gravitational acceleration across the interface  $z = z_d$ ,

$$y_2(z_d) = \left[ g_z(z_d) - \frac{k_x^2}{\sqrt{k_x^2 + k_y^2}} V_{\rm A}^2 \right] y_1(z_d), \qquad (50)$$

and

$$y_4(z_d) = -4\pi G y_1(z_d) + \sqrt{k_x^2 + k_y^2} y_3(z_d).$$
 (51)

The natural boundary conditions at the mid-plane (z = 0) are,

$$\begin{cases} y_1(0) = y_4(0) = 0, & \text{(in the case of symmetry)}, \\ y_2(0) = y_3(0) = 0, & \text{(in the case of antisymmetry)}. \end{cases}$$
(52)

#### 4. RESULTS

In this section we present the dispersion relation of the Parker-Jeans instability with respect to different parameters of the system, such as the CR diffusion coefficient  $\kappa_{\parallel}$ , the initial ratio of the CR pressure to gas pressure  $\beta$ , the initial half-thickness of the gaseous disk  $z_d$ , and the angular velocity  $\Omega$ . We choose  $\alpha = 1$ ,  $\beta = 1$ ,  $z_d/H_0 = 1$ ,  $\kappa_{\parallel}/C_{s0}H_0 = 100$ ,  $\Omega = 0$  as the fiducial model (see § 2 for the normalisations). The values of  $z_d$  and  $\kappa_{\parallel}$  in the following discussion are the normalised values.

We only present the results of symmetric boundary at z = 0, because the growth rate in the case of antisymmetric boundary at z = 0 is much smaller (e.g., Chou et al. 2000).

In the following,  $\sigma_x$  and  $\sigma_{x,\text{max}}$  denote the growth rate and maximum growth rate when  $k_y = 0$ , i.e., no perturbations perpendicular to the unperturbed magnetic field; and  $\sigma_y$  and  $\sigma_{y,\text{max}}$  denote the growth rate and maximum growth rate when  $k_x = 0$ , i.e., no perturbations parallel to the unperturbed magnetic field.  $k_{x,\text{crit}}$  ( $k_{y,\text{crit}}$ ) denotes the critical wavenumber beyond which the system becomes stable (i.e.,  $\sigma_x < 0$ ) when  $k_y = 0$  ( $k_x = 0$ ). We are particular interested in these two perturbations ( $k_y = 0$  and  $k_x = 0$ ), because from the numerically studies we have so far, the most unstable mode of the system always occurs at either  $k_y = 0$  or  $k_x = 0$ . That means the magnetised gaseous disk tends to break up into elongated fragments with axes either perpendicular to ( $k_y = 0$ ) or parallel to ( $k_x = 0$ ) the initial magnetic field.

## 4.1. Dependence on CR Diffusion Coefficient $\kappa_{\parallel}$

Fig. 2 (top) shows the dispersion relation of the case  $k_y=0$  for different  $\kappa_{\parallel}$  (the CR diffusion coefficient). The other parameters take the fiducial values  $\alpha=1,\ \beta=1,\ z_d=1$  and  $\Omega=0$ . As  $\kappa_{\parallel}$  increases, the growth rate  $\sigma_x$  becomes larger and the short wavelength perturbations become more and more unstable. The most unstable mode (the wavenumber at which  $\sigma_x$  attains its maximum value) increases as  $\kappa_{\parallel}$  increases. We note that  $k_{x,\rm crit}$ , the critical wavenumber beyond which the system becomes stable is different for  $\kappa_{\parallel}=0$  and  $\kappa_{\parallel}\neq 0$ . This remind us about the effect of diffusion of CR on Jeans instability of uniform unperturbed state. When CR and gas are tightly bound together, the stability criterion depends on the sum of the gas and CR pressures. If there is CR diffusion (no matter how small it is), the stability criterion depends on the gas pressure only. The only effect of CR is on the growth rate and not the stability criterion.

Fig. 2 (bottom) shows the dependence of the maximum growth rate  $\sigma_{x,\text{max}}$  on  $\kappa_{\parallel}$ .  $\sigma_{x,\text{max}}$  ranges from  $\sim 0.53$  to  $\sim 0.65$  in the range of  $0 < \kappa_{\parallel} < 200$ . When  $\kappa_{\parallel} < 10$ ,  $\sigma_{x,\text{max}}$  increases rapidly with  $\kappa_{\parallel}$ , then it levels off to almost a constant when  $\kappa_{\parallel} > 100$ .

Fig. 3 shows the dispersion relation of the case  $k_x = 0$  for different  $\kappa_{\parallel}$ . The other parameters take the fiducial values  $\alpha = 1$ ,  $\beta = 1$ ,  $z_d = 1$  and  $\Omega = 0$ .  $\sigma_y$  does not depend on  $\kappa_{\parallel}$  at all, which is understandable as CRs diffuse along magnetic field lines only.

Fig. 4 shows the dispersion relation of general perturbations for  $\kappa_{\parallel} = 100$  (left), 1 (middle), and 0.1 (right). The other parameters take the fiducial values  $\alpha = 1$ ,  $\beta = 1$ ,  $z_d = 1$  and  $\Omega = 0$ . Since  $\sigma_{x,\text{max}}$  decreases as  $\kappa_{\parallel}$  decreases while  $\sigma_{y,\text{max}}$  is independent of  $\kappa_{\parallel}$ , it is expected that the most unstable mode shifts from  $k_y = 0$  to  $k_x = 0$  as  $\kappa_{\parallel}$  decreases. In fact, the transition occurs somewhere around  $\kappa_{\parallel} \sim 1$  (Fig. 4 middle). As the coupling between CR and gas increases, the short wavelength perturbations in the unperturbed magnetic field direction are inhibited.

Although the system is stable for large  $k_y$  when  $k_x = 0$ , it is unstable when  $k_x$  is small but not zero. Moreover, the growth rate at large  $k_y$  and small  $k_x$  becomes smaller as  $\kappa_{\parallel}$  decreases.

## 4.2. Dependence on Ratio of CR Pressure to Gas Pressure $\beta$

Fig. 5 shows the dispersion relation of the case  $k_y = 0$  for different  $\beta$  (the ratio of the unperturbed CR pressure to gas pressure). The other parameters take the fiducial values  $\alpha = 1$ ,  $\kappa_{\parallel} = 100$ ,  $z_d = 1$  and  $\Omega = 0$ .  $\sigma_{x,\text{max}}$  increases (decreases) with  $\beta$  when  $\beta < 3$ 

(> 3). The critical wavenumber  $k_{x,\text{crit}}$  increases with  $\beta$  for  $\beta < 3$ , and it remains roughly the same for  $\beta > 3$ . As mentioned in previous subsection that CR should not affect the Jeans stability criterion of uniform unperturbed state when the diffusion coefficient is nonzero. The dependence on  $\beta$  of the critical wavenumber in this case comes from the dependence of the scale height of the unperturbed nonuniform state on the unperturbed CR pressure.

Fig. 6 shows the dispersion relation of the case  $k_x=0$  for different  $\beta$ . The other parameters take the fiducial values  $\alpha=1$ ,  $\kappa_{\parallel}=100$ ,  $z_d=1$  and  $\Omega=0$ .  $\sigma_{y,\text{max}}$  decreases as  $\beta$  increases and levels off at  $\beta>10$ .

Fig. 7 shows the dispersion relation of general perturbations for  $\beta = 1$  (left), 40 (middle), and 100 (right). The other parameters take the fiducial values  $\alpha = 1$ ,  $\kappa_{\parallel} = 100$ ,  $z_d = 1$  and  $\Omega = 0$ . At small  $\beta$  the most unstable mode has  $k_y = 0$ . Around  $\beta \sim 40$ ,  $\sigma_{x,\text{max}} \approx \sigma_{y,\text{max}}$  and the most unstable mode shifts to  $k_x = 0$  for larger  $\beta$ . Moreover, the growth rate at large  $k_y$  and small  $k_x$  decreases slightly as  $\beta$  increases.

## 4.3. Dependence on Half-Thickness $z_d$

Fig. 8 shows the dispersion relation of the case  $k_y = 0$  for different  $z_d$  (the half-thickness of the unperturbed gas disk). The other parameters take the fiducial values  $\alpha = 1$ ,  $\beta = 1$ ,  $\kappa_{\parallel} = 100$  and  $\Omega = 0$ . Both  $\sigma_{x,\text{max}}$  and  $k_{x,\text{crit}}$  increase as  $z_d$  increases.

Fig. 9 shows the dispersion relation of the case  $k_x = 0$  for different  $z_d$ . The other parameters take the fiducial values  $\alpha = 1$ ,  $\kappa_{\parallel} = 100$ ,  $z_d = 1$  and  $\Omega = 0$ . As  $z_d$  increases,  $\sigma_{y,\text{max}}$  gradually increases and  $k_{y,\text{crit}}$  decreases quite a lot.

Fig. 10 shows the dispersion relation of general perturbations for  $z_d = 2$  (left), 0.67 (middle), and 0.35 (right). The other parameters take the fiducial values  $\alpha = 1$ ,  $\beta = 1$ ,  $\kappa_{\parallel} = 100$  and  $\Omega = 0$ . When the  $z_d$  is large (small) the most unstable mode occurs at  $k_y = 0$  ( $k_x = 0$ ). When the perturbations develop into elongated fragments, they prefer to align perpendicular (parallel) to the unperturbed magnetic field. The transition between parallel and perpendicular fragmentation occurs around  $z_d = 0.67$ .

#### 4.4. Dependence on Angular Velocity $\Omega$

Fig. 11 (*left*) shows the dependence of the maximum growth rate on  $\beta$  for different  $\Omega$  (rotational angular velocity of the disk). The other parameters take the fiducial values  $\alpha = 1$ ,  $\beta = 1$ ,  $\kappa_{\parallel} = 100$  and  $z_d = 1$ . We note that the maximum growth rate is mostly

 $\sigma_{x,\text{max}}$  for the cases we studied here. As  $\beta$  increases, the maximum growth rate increases slightly until  $\beta \sim 3$  for  $\Omega = 0.0$ ,  $\beta \sim 5$  for  $\Omega = 0.5$  and  $\beta \sim 9$  for  $\Omega = 1.0$ , then it decreases with  $\beta$ . However, in the case of  $\Omega = 0.0$ , the maximum growth rate shifts to more or less constant at  $\beta > 40$ , because the maximum growth rate shifts from  $\sigma_{x,\text{max}}$  to  $\sigma_{y,\text{max}}$  at  $\beta \sim 40$ . When we increase  $\Omega$ , the shift from  $\sigma_{x,\text{max}}$  to  $\sigma_{y,\text{max}}$  occurs at larger and larger  $\beta$ . When  $\Omega > 0.26$  this shift of unstable modes never substantiates, and the  $k_x = 0$  mode becomes stabilised (see Fig. 11, right). The growth of perturbations in this direction is stabilised by the Coriolis force. Thus when  $\Omega$  is large enough the elongated filaments always align along the unperturbed magnetic field.

#### 5. SUMMARY AND DISCUSSION

This is the first attempt to study how cosmic rays affect the Parker-Jeans instability of magnetized self-gravitating gaseous disks. We adopt a two-fluid model for the cosmic-ray-plasma system, in which the propagation of cosmic rays includes advection and diffusion. In this work we consider slab geometry with magnetic field lies along the slab, and cosmic rays diffuse only along the magnetic field lines. Moreover, we neglect external gravitational force. We perform standard linear perturbation analysis and work out the cases of symmetric boundary conditions at z = 0 (Eq. (52), antisymmetric modes are less unstable). In general the most unstable mode occurs at either  $k_y = 0$  or  $k_x = 0$ , where the unperturbed initial magnetic field lies in the x-direction. Thus the perturbations will develop into elongated fragments with axes either perpendicular to  $(k_y = 0)$  or parallel to  $(k_x = 0)$  the initial magnetic field.

The coupling between CRs and gas is contained in the diffusion coefficient in our model. In the case of  $k_y = 0$ , the growth rate of the instability increases as  $\kappa_{\parallel}$  increases (i.e., the coupling becomes weaker), and is levelled off at large  $\kappa_{\parallel}$  (see Fig. 2). Recall that the thermal gas pressure is the stabilizing factor in both Jeans instability and Parker instability. One may interpret CR as a gas that can slip through the thermal gas according to the value of the diffusion coefficient or the strength of the coupling. During the process it exerts part of its pressure onto the thermal gas. In effect the thermal gas pressure is augmented and the Parker-Jeans instability becomes less unstable. We should point out that the instability cannot be stabilized by just decreasing the diffusion coefficient (it is less unstable only), except when the diffusion coefficient is exactly zero and the CRs and thermal gas are tightly bound together. See Fig. 2 (top) for detail. In the case of  $k_x = 0$ , the dispersion relation does not depend on  $\kappa_{\parallel}$  (see Fig. 3). This reflects the assumption that CRs diffuse along the magnetic field lines only.

Keeping other parameters fixed, the increase of  $\beta$  (the ratio of unperturbed CR pressure to gas pressure) has both stabilizing and destabilizing effect (see Fig. 5). The wavenumber beyond which the system is stable increases as  $\beta$  increases (it approaches a maximum value when  $\beta > 3$ ), i.e., the unstable range increases. The maximum growth rate increases (slightly) with  $\beta$  when  $\beta < 3$  but decreases with  $\beta$  when  $\beta > 3$ . We deem that the Parker mode is responsible for the increase in the unstable range and also for the increase in maximum growth rate when  $\beta < 3$ , while the Jeans mode is responsible for the decrease in maximum growth rate when  $\beta > 3$ . For comparison, Parker instability under constant external gravity (and no self-gravity is considered) is usually studied in an exponential atmosphere. As  $\beta$  increases, both unstable range and maximum growth rate increase until some maximum values (see the appendix for a brief discussion). The effect of CRs on Parker instability under constant external gravity has, of course, been studied before, for instance, the original work by Parker (1966), and more recent works by Ryu et al. (2003) and Kuwabara et al. (2004) which have taken the diffusion of CR into account. However, one may notice that in Parker (1966) and Ryu et al. (2003), both unstable range and maximum growth rate of the instability increase without limit as  $\beta$  approaches  $\infty$ . We should point out that the apparent increase without bound is just an artefact of normalisation. In these works the wavenumber and the growth rate are normalised to 1/H and u/H, where H is the scale height of the exponential atmosphere which is proportional to the total unperturbed pressure, and u is a characteristic speed (say, the isothermal sound speed). Thus the normalisation decreases as  $\beta$  increases. The actual unstable range and maximum growth rate are always finite (see appendix).

Nagai et al. (1998) showed that the direction of the longitudinal axis of the elongated filaments formed by the growth of the perturbation with respect to the magnetic field depends on the half thickness of the disk or the external pressure. For thicker (thinner) disk the growth rate of perturbations in the x direction is larger (smaller) than those in the y direction. Here we demonstrate that the alignment can also be affected by CR diffusion. Fig. 12 shows the dependence of the growth rate on the half thickness of the disk  $z_d$  and the relation between  $\sigma_{x,\max}$  and  $\sigma_{y,\max}$  for different  $\kappa_{\parallel}$  in the case of  $\alpha=1$  and  $\beta=1$ . As long as  $\sigma_{x,\max}<\sigma_{y,\max}$  the filaments will align along the magnetic field. As shown in the figure, when  $z_d<0.65$  or  $z_d>1.1$ , then  $\sigma_{x,\max}$  is either always smaller or larger than  $\sigma_{y,\max}$  and the diffusion of CR does not affect the direction of the filaments. However, when  $0.65 < z_d < 1.1$  (the grey region in the figure), the alignment depends on  $\kappa_{\parallel}$ . At a particular  $z_d$  the filaments prefer to align along the magnetic field when  $\kappa_{\parallel}$  is small enough (i.e., the coupling is strong enough), and vice versa.

The CR pressure also affect the alignment of filaments. Fig. 13 shows the dependence of the growth rates  $\sigma_{x,\text{max}}$  and  $\sigma_{y,\text{max}}$  on  $\beta$  for three thickness  $z_d = 3$ , 1, and 0.66. Whenever

there is a crossover between the curves  $\sigma_{x,\text{max}}$  and  $\sigma_{y,\text{max}}$  for the same  $z_d$ , the direction of the filaments depends on the CR pressure. In the case of  $z_d = 0.66$ ,  $\sigma_{x,\text{max}}$  is always smaller than  $\sigma_{y,\text{max}}$ . For  $z_d = 1$  and  $z_d = 3$ ,  $\sigma_{x,\text{max}} < \sigma_{y,\text{max}}$  when  $\beta > 40$  and  $\beta > 550$ , respectively (also see Fig. 7 for the case of  $z_d = 1$ ). In fact, for larger  $z_d$  crossover still exists for large enough  $\beta$ , but the difference between  $\sigma_{x,\text{max}}$  and  $\sigma_{y,\text{max}}$  is very small in those range of  $\beta$ . Therefore, the alignment of the elongated filament depends on CR pressure when the thickness of the disk is large enough ( $z_d > 0.66$ ).

The dependence of the eigenfunction  $\delta \bar{\rho}$  on several factors is shown in Fig. 14. The top panel shows the dependence on the CR diffusion coefficient  $\kappa_{\parallel}$ . The solid line shows  $\delta \bar{\rho}$  with  $\kappa_{\parallel} = 200$  at the most unstable wave number  $(k_x, k_y) = (0.5, 0)$ , and the dotted line shows  $\delta \bar{\rho}$  with any  $\kappa_{\parallel} < 1$  at the most unstable wave number  $(k_x, k_y) = (0, 0.35)$ . The middle panel shows the dependence on the half thickness of the disk  $z_d$ . The solid line shows the  $\delta \bar{\rho}$  with  $z_d = 3$  at the most unstable wave number  $(k_x, k_y) = (0.59, 0)$  and the dotted line shows  $\delta \bar{\rho}$  with  $z_d = 0.1$  at the most unstable wave number  $(k_x, k_y) = (0, 2.94)$ . The bottom panel shows the dependence on the ratio of CR pressure to gas pressure  $\beta$ . The solid line shows the  $\delta \bar{\rho}$  with  $\beta = 3$  at the most unstable wave number  $(k_x, k_y) = (0.51, 0)$  and the dotted line shows  $\delta \bar{\rho}$  with  $\beta = 1000$  at the most unstable wave number  $(k_x, k_y) = (0, 0.29)$ . The solid line in each panel shows the case when the elongated filaments have the tendency to align their longitudinal axes perpendicular to the unperturbed magnetic field, while the dotted line in each panel shows the case when the elongated filaments prefer to align along the unperturbed magnetic field. Fig. 14 shows that the perturbation of density concentrate around the mid-plane if the most unstable mode is  $k_x = 0$  (the dotted line), while it spread more evenly if the most unstable mode is  $k_y = 0$  (the solid line).

Numerical computations were carried out on the VPP5000 at the National Astronomical Observatory, Japan (NAOJ) under the projects wtk03b, and the SX-6 at the National institute of Information and Communications Technology (NICT), Japan. C.M. Ko is supported in part by the National Science Council of Taiwan, by grants NSC-92-2112-M-008-046 and NSC-93-2112-M-008-017.

#### A. PARKER INSTABILITY IN AN EXPONENTIAL ATMOSPHERE

In this appendix we briefly describe the dependence of the unstable range and the maximum growth rate of the Parker instability under constant external gravity in an exponential atmosphere.

In the unperturbed equilibrium state the external gravity  $\mathbf{g} = -g\mathbf{e}_{\mathbf{z}}$  and the magnetic

field  $\mathbf{B} = B\mathbf{e}_{\mathbf{x}}$ . The hydrostatic equilibrium equation (g is constant)

$$\frac{\mathrm{d}P_{\mathrm{t}}}{\mathrm{d}z} = -\rho g\,,\tag{A1}$$

gives an exponential atmosphere if  $P_{\rm t} \propto \rho$ . Specifically,  $P_{\rm t} = P_{\rm t0} \exp[-z/H]$  and  $\rho = \rho_0 \exp[-z/H]$ . The scale height  $H = P_{\rm t}/(\rho g) = P_{\rm t0}/(\rho_0 g)$  is a constant. The total pressure  $P_{\rm t}$  includes thermal gas pressure, magnetic pressure and other pressures such as cosmic ray pressure.

To study the linear stability of the system, one may perform standard normal mode analysis. We present the result of a particular simple case: only gas and magnetic field are actively involved in the dynamics of the system. The other components, e.g., cosmic rays, just provide the background pressure against the external gravity in the unperturbed equilibrium state. This is the case when cosmic ray diffusion coefficient is very large, i.e., the coupling is vanishing small. Let the perturbations be proportional to  $\exp(\sigma t + ik_x x)$  (forget about perturbations in y-direction to further simplify discussion). The dispersion relation of the lowest mode in z-direction is

$$\sigma^4 + \left(V_{\rm A}^2 + C_{\rm s}^2\right) \left(k_x^2 + \frac{1}{4H^2}\right) \sigma^2 + k_x^2 C_{\rm s}^2 \left[ \left(k_x^2 + \frac{1}{4H^2}\right) V_{\rm A}^2 + N^2 \right] = 0, \tag{A2}$$

where  $V_{\rm A}=B/\sqrt{\mu_0\rho}$  and  $C_{\rm s}=\sqrt{\gamma_{\rm g}P_{\rm g}/\rho}$  are the Alfvén velocity and adiabatic sound speed, respectively;  $N=\sqrt{g/H-g^2/C_{\rm s}^2}$  is the Brunt-Väisäläa frequency (with contributions from magnetic field and cosmic rays through H). The system is susceptible to Parker instability if

$$N^{2} + \frac{V_{\rm A}^{2}}{4H^{2}} = \frac{g}{H} - \frac{g^{2}}{C_{\rm c}^{2}} + \frac{V_{\rm A}^{2}}{4H^{2}} < 0.$$
 (A3)

To facilitate discussion, we suppose  $P_{\rm B}=B^2/2\mu_0=\alpha P_{\rm g}$ ,  $P_{\rm c}=\beta P_{\rm g}$  and  $P_{\rm g}=\rho u^2$  (the isothermal sound speed u is constant). Thus  $P_{\rm t}=P_{\rm g}+P_{\rm B}+P_{\rm c}=(1+\alpha+\beta)P_{\rm g}=(1+\alpha+\beta)\rho u^2$ . A natural time scale of the system is u/g and a natural length scale is  $u^2/g$ . In these units the parameters in Eq. (A2) become:  $V_{\rm A}^2=2\alpha$ ,  $C_{\rm s}^2=\gamma_{\rm g}$ ,  $H=(1+\alpha+\beta)$  and  $N^2=-(1+\alpha+\beta-\gamma_{\rm g})/(1+\alpha+\beta)/\gamma_{\rm g}$ . The growth rate and wavenumber become  $\sigma u/g$  and  $k_x u^2/g$ . The instability criterion Eq. (A3) can then be written as (cf., Parker 1966)

$$(1 + \alpha + \beta)^2 > \gamma_g \left( 1 + \frac{3}{2}\alpha + \beta \right) . \tag{A4}$$

In these units it can readily be shown that the critical wavenumber beyond which the system is stable is given by

$$\left(k_{x,\text{crit}}\frac{u^2}{g}\right)^2 = \frac{1}{2\alpha\gamma_g} \left[1 - \frac{\gamma_g\left(1 + \frac{3}{2}\alpha + \beta\right)}{(1 + \alpha + \beta)^2}\right], \tag{A5}$$

and the maximum growth rate is given by the smaller root of

$$(2\alpha - \gamma_{g}) \left(\sigma_{x,\max} \frac{u}{g}\right)^{4} - 2(2\alpha + \gamma_{g}) \left[1 - \frac{\gamma_{g} \left(1 + \frac{1}{2}\alpha + \beta\right)}{(1 + \alpha + \beta)^{2}}\right] \left(\sigma_{x,\max} \frac{u}{g}\right)^{2} + \left[1 - \frac{\gamma_{g} \left(1 + \frac{3}{2}\alpha + \beta\right)}{(1 + \alpha + \beta)^{2}}\right]^{2} = 0.$$
(A6)

In fact,  $(k_{x,\text{crit}}u^2/g)^2$  and  $(\sigma_{x,\text{max}}u/g)^2$  increase monotonically with  $\beta$ . Moreover, as  $\beta \to \infty$ ,  $(k_{x,\text{crit}}u^2/g)^2 \to 1/2\alpha\gamma_g$  and  $(\sigma_{x,\text{max}}u/g)^2 \to 1/(\sqrt{2\alpha} + \sqrt{\gamma_g})$ .

## REFERENCES

Berezinskii, V. S., Bulanov, S. V., Dogiel, V. A., Ginzburg, V. L., & Ptuskin, V. S. 1990, Astrophysics of Cosmic Rays, ed. V. S. Verezinskii & V. L. Ginzburg (New York: North-Holland)

Chou, W., Matsumoto, R., Tajima, T., Umekawa, M., & Shibata, K. 2000, ApJ, 538, 710

Drury, L.O'C. 1983, Rep. Prog. Phys., 46, 973

Drury, L.O'C., & Völk, H. J. 1981, ApJ, 248, 344

Elmegreen, B. G., & Elmegreen, D. M. 1978, ApJ, 220, 1051

Elmegreen, B. G. 1982a, ApJ, 253, 634

Elmegreen, B. G. 1982b, ApJ, 253, 655

Ferrière, K. M. 2001, RMP, 73, 1031

Gaisser, T. K. 1990, Cosmic Rays and Particle Physics (Cambridge: Cambridge University Press)

Giacalone, J., & Jokipii, J. R. 1999, ApJ, 520, 204

Hanasz, M. 1997, A&A, 327, 813

Hanasz, M., & Lesch, H. 1997, A&A, 321, 1007

Hanasz, M., & Lesch, H. 2000, ApJ, 543, 235

Hanasz, M., & Lesch, H. 2003, A&A, 412, 331

Hanasz, M., Kosinski, R., & Lesch, H. 2004, Ap&SS, 289, 303

Hanasz, M., Kowal, G., Otmianowska-Mazur, K., & Lesch, H. 2004, ApJ, 605, L33

Hanawa, T., Nakamura, F., & Nakano, T. 1992, PASJ, 44, 509

Kim, J., Hong, S. S., & Ryu, D. 1997, ApJ, 485, 228

Kim, J., Hong, S. S. 1998, ApJ, 507, 254

Kim, W. T., Ostriker, E. C., & Stone J. M. 2002

Ko, C. M. 1992, å, 259, 377

Kuwabara, T., Nakamura, K., & Ko, C. M., ApJ, 607, 828

Lee, S. M., & Hong, S. S. 2005, Arxiv, http://arxiv.org/abs/astro-ph/0503013

Lee, S. M., Hong, S. S., & & Kim, J. 2001, JKAS, 34, L285

Nagai, T., Inutsuka, S., & Miyama, M. 1998, ApJ, 506, 306

Paker, E. N. 1996, ApJ, 145, 811

Ptuskin, V. S. 2001, Space Sci. Rev., 99, 281

Ryu, D., Kim, J., Hong, S. S., & Jones, T. W. 2003, ApJ, 589, 338

This preprint was prepared with the AAS LATEX macros v5.0.

- Fig. 1.— Left: Gas pressure in the unperturbed equilibrium state as a function of z (vertical coordinate) in the case of  $\alpha = 1$  and  $\beta = 1$ . Right: Gravity in the unperturbed equilibrium state as a function of z.
- Fig. 2.— Top: The dependence of the dispersion relation at  $k_y = 0$  on  $\kappa_{\parallel}$ , the CR diffusion coefficient.  $\sigma_x$  is the growth rate when  $k_y = 0$  and  $k_x$  is the wavenumber in the direction of the unperturbed magnetic field. The other parameters are  $\alpha = 1$ ,  $\beta = 1$ ,  $z_d = 1$  and  $\Omega = 0$ . Bottom: The dependence of the maximum growth rate  $\sigma_{x,\text{max}}$  on  $\kappa_{\parallel}$ .
- Fig. 3.— The dependence of the dispersion relation at  $k_x = 0$  on  $\kappa_{\parallel}$ .  $\sigma_y$  is the growth rate when  $k_x = 0$ . The other parameters are the same as in Fig. 2.
- Fig. 4.— The general dispersion relation for the Parker-Jeans instability against the effect of CR diffusion. Left:  $\kappa_{\parallel} = 100$ , Middle:  $\kappa_{\parallel} = 1$ , and Right:  $\kappa_{\parallel} = 0.1$ . The other parameters are the same as in Fig. 2.
- Fig. 5.— The dependence of the dispersion relation at  $k_y = 0$  on  $\beta$ , the ratio of the unperturbed CR pressure to gas pressure.  $\sigma_x$  is the growth rate when  $k_y = 0$ . The other parameters are  $\alpha = 1$ ,  $\kappa_{\parallel} = 100$ ,  $z_d = 1$  and  $\Omega = 0$ .
- Fig. 6.— The dependence of the dispersion relation at  $k_x = 0$  on  $\beta$ .  $\sigma_y$  is the growth rate when  $k_x = 0$ . The other parameters are the same as in Fig. 5.
- Fig. 7.— The general dispersion relation for the Parker-Jeans instability against the effect of CR pressure. Left:  $\beta = 1$ , Middle:  $\beta = 40$ , and Right:  $\beta = 100$ . The other parameters are the same as in Fig. 5.
- Fig. 8.— The dependence of the dispersion relation at  $k_y = 0$  on  $z_d$ , the half-thickness of the unperturbed gas disk (can be viewed as a measure of external pressure).  $\sigma_x$  is the growth rate when  $k_y = 0$ . The other parameters are  $\alpha = 1$ ,  $\beta = 1$ ,  $\kappa_{\parallel} = 100$  and  $\Omega = 0$ .
- Fig. 9.— The dependence of the dispersion relation at  $k_x = 0$  on  $z_d$ .  $\sigma_y$  is the growth rate when  $k_x = 0$ . The other parameters are the same as in Fig. 8.
- Fig. 10.— The general dispersion relation for the Parker-Jeans instability against the effect of the half-thickness of the gas disk. Left:  $z_d = 2$ , Middle:  $z_d = 0.67$ , and Right:  $z_d = 0.35$ . The other parameters are the same as in Fig. 8.

Fig. 11.— Left: The dependence of the maximum growth rate  $\sigma_{\rm max}$  on  $\beta$  (the ratio of unperturbed CR pressure to gas pressure) at different angular velocity of the gas disk  $\Omega$ . The other parameters are  $\alpha=1,\ \beta=1,\ \kappa_{\parallel}=100$  and  $z_d=1$ . Right: The general dispersion relation in the case of  $\alpha=1,\ \beta=1,\ \kappa_{\parallel}=100,\ z_d=1$  and  $\Omega=0.5$ 

.

Fig. 12.— The dependence of the maximum growth rate on the half-thickness  $z_d$ .  $\sigma_{x,\text{max}}$  is the maximum growth rate at  $k_y = 0$  at a given  $\kappa_{\parallel}$ .  $\sigma_{y,\text{max}}$  is the maximum growth rate at  $k_x = 0$  ( $\sigma_{y,\text{max}}$  is independent of  $\kappa_{\parallel}$ , see Fig. 3). The other parameters are  $\alpha = 1$ ,  $\beta = 1$  and  $\Omega = 0$ . In the grey region, CR diffusion determines which mode is more unstable, thus determines the alignment of the perturbations with respect to the unperturbed magnetic field.

Fig. 13.— The dependence of the maximum growth rate on the ratio of CR pressure to gas pressure  $\beta$  at different  $z_d$ . The other parameters are  $\alpha = 1$ ,  $\kappa_{\parallel} = 100$  and  $\Omega = 0$ .

Fig. 14.— The eigenfunction  $\delta\bar{\rho}$  of the most unstable mode. Top: The dependence on the CR diffusion coefficient  $\kappa_{\parallel}$ . The solid line is the case of  $\kappa_{\parallel}=200$  at the wavenumber  $(k_x,k_y)=(0.5,0)$ , and the dotted line is the case of any  $\kappa_{\parallel}<1$  at the wavenumber  $(k_x,k_y)=(0,0.35)$ . The other parameters are  $\alpha=1$ ,  $\beta=1$ ,  $z_d=1$  and  $\Omega=0$ . Middle: The dependence on the half-thickness  $z_d$ . The solid line is the case of  $z_d=3$  at  $(k_x,k_y)=(0.59,0)$ , and the dotted line is the of  $z_d=0.1$  at  $(k_x,k_y)=(0,2.94)$ . The other parameters are  $\alpha=1$ ,  $\beta=1$ ,  $\kappa_{\parallel}=100$  and  $\Omega=0$ . Bottom: The dependence on the ratio of CR pressure to gas pressure  $\beta$ . The solid line is the case of  $\beta=3$  at  $(k_x,k_y)=(0.51,0)$ , and the dotted line shows the case of  $\beta=1000$  at  $(k_x,k_y)=(0,0.29)$ . The other parameters are  $\alpha=1$ ,  $\kappa_{\parallel}=100$ ,  $z_d=1$  and  $\Omega=0$ .

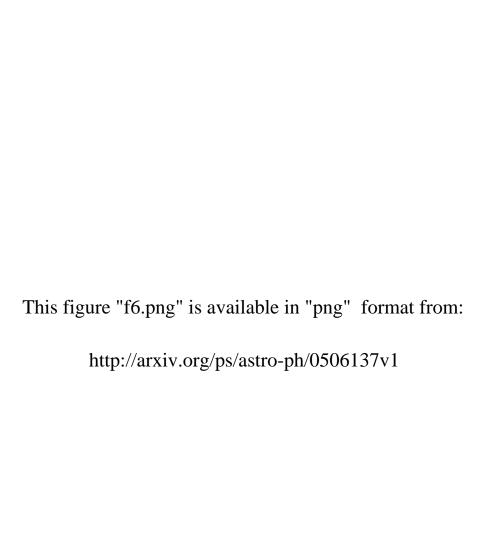
This figure "f1.png" is available in "png" format from:

This figure "f2.png" is available in "png" format from:

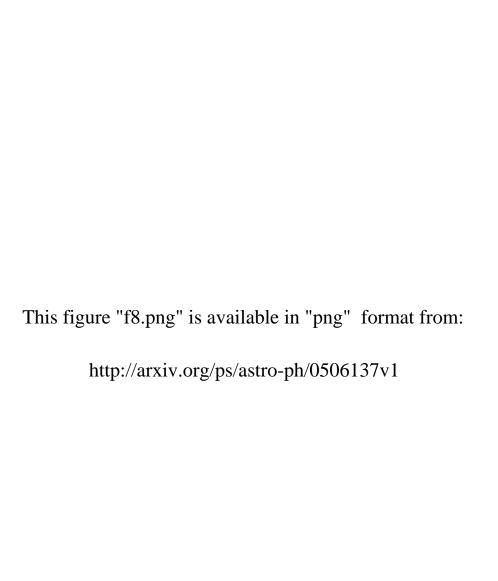
This figure "f3.png" is available in "png" format from:

This figure "f4.png" is available in "png" format from:

This figure "f5.png" is available in "png" format from:



This figure "f7.png" is available in "png" format from:



This figure "f9.png" is available in "png" format from:

This figure "f10.png" is available in "png" format from:

This figure "f11.png" is available in "png" format from:

This figure "f12.png" is available in "png" format from:

This figure "f13.png" is available in "png" format from:

This figure "f14.png" is available in "png" format from: